The Astrophysical Journal, 599:615–625, 2003 December 10

FLARE-RELATED MAGNETIC ANOMALY WITH A SIGN REVERSAL

Jiong Qiu and Dale E. Gary
Center For Solar Research, Department of Physics, New Jersey Institute of Technology,
323 Martin Luther King Boulevard, Newark, NJ 07102-1982; qiuj@plage.njit.edu
Received 2002 April 25; accepted 2003 August 18

ABSTRACT

In this paper we report a significant magnetic anomaly, specifically an apparent sign reversal of magnetic polarities in small areas of Michelson Doppler Imager (MDI) magnetograms during the impulsive phase of an X5.6 flare on 2001 April 6. Three flare kernels were observed to emit $\geq$50 keV hard X-rays, which are located in strong magnetic fields of order $\pm$1000–1500 G. We find that the apparent sign reversal began and persisted for a few minutes in all three kernels, in precise temporal and spatial correspondence with the hard X-ray sources. We search for a combination of instrumental and flare-induced line profile effects that can account for this behavior. Our studies provide a viable scenario that the observed transient sign reversal is likely to be produced by distorted measurements when the Ni I 6768 Å line comes into emission or strong central reversal as a result of nonthermal beam impact on the atmosphere in regions of strong magnetic fields.

Subject headings: Sun: activity — Sun: flares — Sun: magnetic fields — Sun: X-rays, gamma rays

1. INTRODUCTION

The changes in magnetic fields that are caused by or related to solar flares have been discussed and debated for decades. Significant effort has been made in searching for observational evidence of magnetic field changes related to solar flares (for a review see Sakurai & Hiei 1996), and some recent observations show the indications of magnetic field changes in at least some large flare events, e.g., X-class flares (Kosovichev & Zharkova 2001; Wang et al. 2002). The observations reveal two kinds of changes. A "permanent" change is defined as an irreversible change in the measured magnetic field from the preflare state to the postflare state. It is usually in the form of flux emergence or flux cancellation and is regarded as a real change in the magnetic field. A "transient" change takes place only during a flare, with the measured magnetic fields resuming the preflare state after the event; hence, it is difficult to interpret the observed transient change as due to real magnetoelectric signals. For this reason, in the following text we term the previously called "magnetic transient" (Patterson 1984; Kosovichev & Zharkova 2001) as a "magnetic anomaly."

Concerning the mechanism of the magnetic anomaly, the general belief is that the measurements of the magnetic fields during flares are significantly distorted. Such distortion can be ascribed either to unusual conditions of the flare atmosphere, such as motion or heating, that greatly modify the line profile or to instrumental problems such as saturation (nonlinearity in the instrument response to strong magnetic fields), scattered light (which can dominate in the dark regions of sunspot umbrae), and, specifically for the Michelson Doppler Imager (MDI), the breakdown of the onboard algorithm when irregular or abnormal line profiles are encountered (Liu & Norton 2001[1]). Both effects will lead to the measured magnetic field being much weaker than the actual field strength.

In some extreme cases, the magnetic anomaly takes the form of a sign reversal; i.e., the measured magnetic fields are temporarily changed to the opposite polarities. The magnetic anomaly in the form of the sign reversal was occasionally observed in large flares at Big Bear Solar Observatory (BBSO) yet less often discussed (H. Wang 2002, private communication). An X-class flare was observed on 1981 June 24, which was accompanied by a prominent magnetic anomaly (Zirin & Tanaka 1981; Patterson & Zirin 1981). Specifically, magnetic sign reversals occurred at several sites inside the flare-inflicted active region. Because BBSO observed the magnetic fields using a single bandpass, the sign reversal was interpreted as due to the lower atmosphere being heated to such an extent that the normally absorptive Fe I λ5324 line came into emission (Patterson 1984). This is, to our knowledge, the only study of the apparent magnetic sign reversal that is available in literature.

Recently an X-class flare was observed by various instruments on 2001 April 6. The magnetograms obtained by MDI show magnetic anomalies during the flare and, specifically, transient sign reversals at various locations during the impulsive phase. The coordinated observations further reveal that these sign-reversed anomalies are exactly coaligned with the high-energy hard X-ray sources, which is most convincing evidence that the sign-reversed anomalies are associated with nonthermal beams. The question is, what is the nature of this association? In this paper we look further into the sign-reversed magnetic anomalies observed in this event and seek to determine the mechanism that is responsible.

We have two motivations for studying this data set. First, all previously observed sign reversals have been associated with flares, indicating that the distorted measurements are related to a physical process in the solar atmosphere. The fact that the reversals we observe are so well correlated with hard X-rays leads us to try to find out what is this specific process. For example, if the sign reversal is produced by distorted measurements on line profiles modified by flare impact, certain circumstances should be met in order to significantly change the line shape. The suggestion that the line should go into emission (e.g., Patterson 1984) sets a very demanding criterion for the atmosphere's reaction to the flare energy release. Specifically, the Ni I 6768 Å line used by

[1] See http://soi.stanford.edu/general/TechNotes/01.144/TN01-144.pdf.

MDI is formed in the temperature minimum region (Jones 1989; Bruls 1993) and is stable against temperature changes (Bruls 1993). Bruls (1993) has shown that in a thermal model, while an increasing temperature can enhance the continuum emission, the formation of the line is dominated by non-LTE processes so that the line may be hardly affected. Obviously, there is no easy way to significantly enhance the source function at the line center by a sudden increase in the temperature of the lower atmosphere. The second motivation for using this data set is that the MDI data are obtained with a well-defined algorithm, with which it is possible to simulate the output signal of MDI in response to a changing line profile. The MDI algorithm uses filtergrams taken at five different positions along the Ni I 6768 Å line, which are then used to calculate the line shifts with a Fourier tachometer method (Scherrer et al. 1995; Kosovichev & Zharkova 2001). Our simulation will also explore the effects of a velocity field and the extent of the saturation problem, which will help us understand whether these effects alone might produce the apparent sign reversal.

In § 2 we present observations of the strong, sign-reversed magnetic anomaly in the 2001 April 6 event, along with other related emissions in EUV, hard X-rays, and microwaves. We make a simple simulation of the MDI measurements to help understand the role of a modified Ni I line profile in producing the magnetic anomaly (§ 3). We also analyze the hard X-ray observations to deduce the energy flux deposited at the locations of the anomaly and discuss the probable mechanisms for the flare-related magnetic anomaly (§ 4). In § 5 we discuss effects of saturation and velocity field on MDI measurements. The conclusions are given in § 6.

2. OBSERVATIONS OF MAGNETIC ANOMALY

The X5.6 flare is among the largest events to occur during solar cycle 23. In this paper we analyze magnetic observations by the MDI (Scherrer et al. 1995) on board *SOHO* and hard X-ray observations by the Hard X-Ray Telescope (HXT; Kosugi et al. 1991) on board *Yohkoh*. Also presented as context observations are EUV images by the *Transition Region and Coronal Explorer* (*TRACE*; Handy et al. 1999) and microwave data by the Owens Valley Solar Array (OVSA; Gary & Hurford 1990). Images obtained at different wavelengths are co-aligned using the pointing information of the instruments.

Figure 1 shows the contours of the hard X-ray emission from the two HXT channels, M2 (33–53 keV) and H (53–93 keV), observed at the flare maximum, which are superposed on the snapshot of the postflare EUV image obtained by *TRACE* and the longitudinal magnetogram by MDI, respectively. The figure illustrates the complex morphology of the flare during the impulsive phase. It is shown that the hard X-ray emission at $\geq$50 keV primarily comes from the footpoints of the SXR/EUV loops. Specifically, we recognize three flare kernels, K1, K2, and K3, which are denoted in the figure, as thick-target hard X-ray sources (Qiu, Lee, & Gary 2003). Notably all three kernels are found inside the sunspot umbrae in the active region.

Figure 1*b* reveals a peculiar observation by MDI, in that at the locations of the hard X-ray emission K1, K2, and K3, the longitudinal magnetic fields exhibit a polarity reversal with respect to the background magnetic fields. In Figure 2 the consecutive series of magnetograms obtained by MDI before, during, and after the flare indicate that the polarity reversal is a transient phenomenon during the impulsive phase of the flare. To demonstrate the flare-related reversal, we superpose on Figure 2*d* the intensity profiles of the magnetic fields along an axis crossing kernels K2 and K3. The white and dark profiles show the magnetic fields an hour before and after the flare, respectively, and the thick gray profiles show the magnetic fields at the flare maximum. It is seen that at locations except flare kernels, there is no significant change in the magnetic fields before, during, and after the flare. However, at flare kernels K2 and K3, apparently the sign of the magnetic fields is reversed. Note that the sign reversal occurred only when/where the footpoint hard X-ray emission is observed (Fig. 1*b*). It is, therefore, logical to consider that the sign-reversed magnetic anomaly in this event is closely related to electron precipitation into the lower atmosphere.

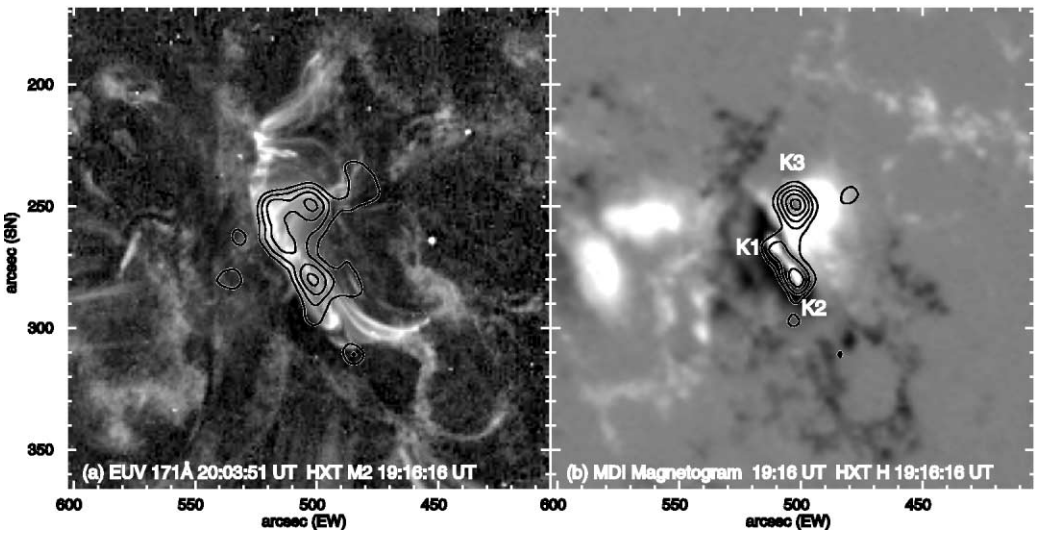

FIG. 1.—(*a*) Filtergram at EUV 171 Å by *TRACE* showing the postflare configuration, superposed with the hard X-ray contours from the HXT M2 channel (33–53 keV). (*b*) Magnetogram by MDI superposed with the hard X-ray contours from the HXT H channel (53–93 keV).

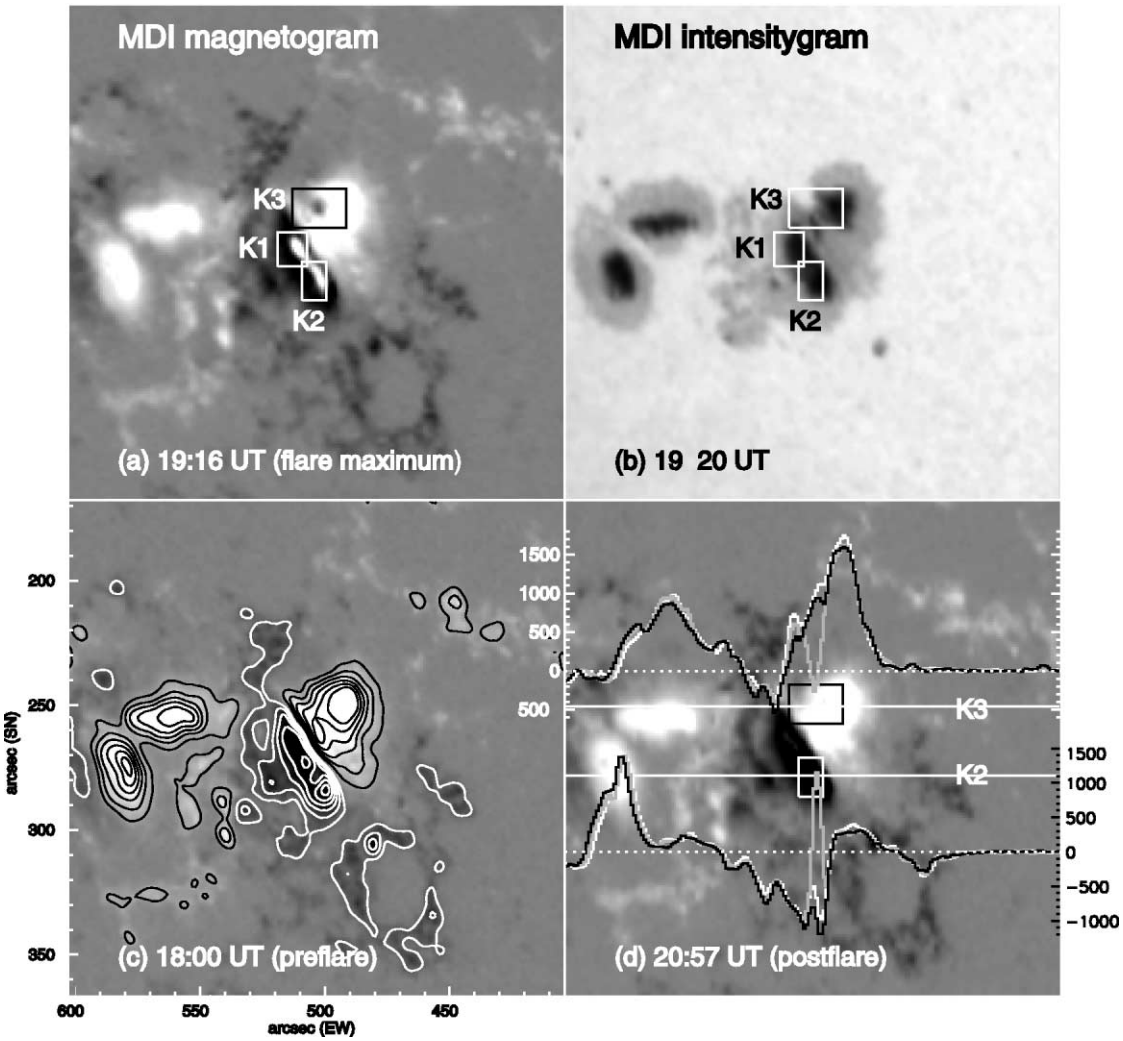

FIG. 2.—(*a*) MDI magnetogram at the maximum of the flare showing magnetic anomaly with a sign reversal at the flare kernels K1, K2, and K3. (*b*) MDI intensity map with the locations of the magnetic transients indicated by three boxes. (*c*) Preflare magnetogram obtained by MDI, the dark/white contours indicating the longitudinal magnetic field strength at ±200, 400, 600, 800, 1000, and 1200 G. (*d*) Postflare magnetogram obtained by MDI, superposed with the profiles of the measured magnetic field strength along the white solid horizontal lines crossing K2 and K3 kernels (as denoted by the white boxes), respectively. The white and black profiles indicate the magnetic field strength before (18:00 UT) and after (20:56 UT) the flare, respectively, and the gray profiles show the apparent magnetic field at 19:16 UT, the maximum of the flare emission. The values for the *Y*-axis give the magnetic field strength in Gauss, and the white dotted horizontal lines indicate the level of zero Gauss.

Figure 2*d* also shows evidence of saturation of the magnetic field measurements inside sunspot umbrae. Seen from the preflare and postflare (white and dark) profiles, toward the center of the umbrae, especially in K2, while the real magnetic field strength should grow to be around −2000 G, the measured field strength actually weakens to only −500 G, which is weaker than the surrounding fields. Figure 3 shows the enlarged magnetograms before and after the flare to further illustrate the pattern of apparent weakening in the umbral regions. Liu & Norton (2001) determined that for the magnetograms taken by MDI, such a specific "saturation" pattern is caused mainly by failure of the onboard algorithm due to low light intensity in umbral regions, and measurement errors also occur because in umbral regions the Ni I line profile shows an evident blend near the line center.

The specific saturation effects occur in the umbral regions very close to where the sign reversal takes place. However, since these saturation effects are persistent in all the magnetograms, they alone do not lead to an anomalous sign reversal in the absence of the flare. Some other mechanisms related to the flare have to be invoked to explain the observed sign reversal.

We also examine the Dopplergrams obtained by MDI. Figure 4 shows the velocity contours superposed on the longitudinal magnetograms taken before (Fig. 4*a*), during (Figs. 4*b*–4*e*), and after (Fig. 4*f*) the flare. Overall the upward velocity dominates the observed active region. From 19:15 to 19:16 UT, temporary downward velocities are observed around the flare kernels, but they do not exactly overlap with the areas of the magnetic sign reversal. In addition, the downflow is observed in a much smaller area than the magnetic anomaly.

The apparent magnetic anomaly not only corresponds spatially to hard X-ray sources, it also bears a close temporal association with the flare emission. In Figure 5*a* we compare the hard X-ray and microwave light curves with the time profiles of the magnetic field change in a few regions that exhibit the sign reversal during the flare. Three regions of interest are marked in Figure 2*b*, which encompass the

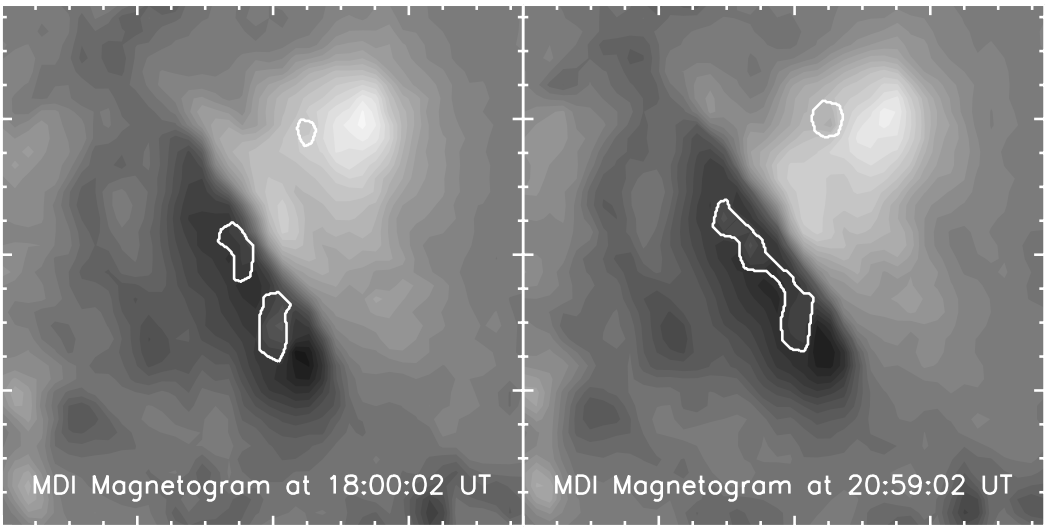

FIG. 3.—MDI magnetograms before and after the flare. The thick white contours indicate sites of saturation effects that lead to apparent weakening of the measured magnetic fields in umbral areas. Note that the field of view of the figures is smaller than in Fig. 2.

flare kernels K1, K2, and K3. To demonstrate the magnetic field sign reversal, we integrate the absolute magnetic flux in each region only over the pixels that exhibit the sign reversal during the flare. The so-derived "magnetic reversal flux" in the three kernels is plotted in Figure 5*b*. Note that in K1 and K2 the original magnetic fields are negative and the "reversal flux" is positive, and vice versa in the case of K3.

Figure 5*b* shows that the evolution of the magnetic anomaly is very similar to the hard X-ray time profiles during the impulsive phase. We note that the sign reversal is delayed in K3 with respect to K1 and K2. This is related to the fact that during the impulsive phase, K3, as seen in hard X-ray images, evolves from near the magnetic neutral line into the umbra, and the sign reversal does not occur until K3 evolves into the strong magnetic fields of $\geq$1000 G. As we will discuss later, however, we believe that the sign reversal requires not only a strong magnetic field but also the weak continuum found in the associated sunspot umbra. Note that during the

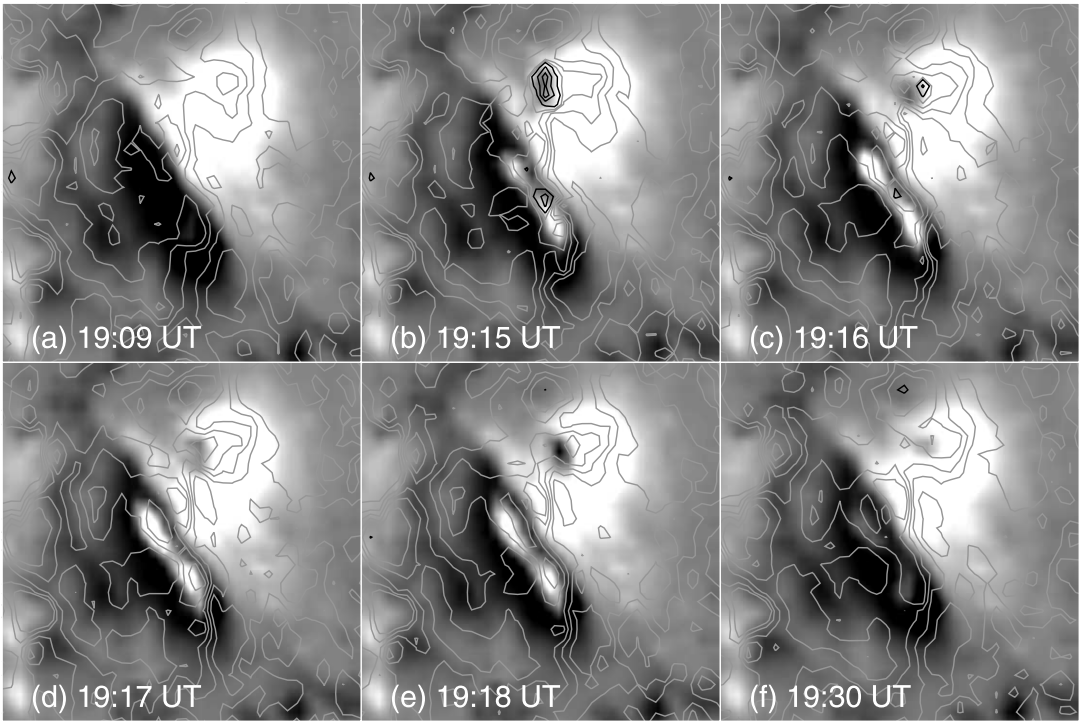

FIG. 4.—MDI magnetograms (*a*) before, (*b*, *c*, *d*, *e*) during, and (*f*) after the flare superposed with the velocity contours. The gray contours indicate upward velocities with the contour levels of 200, 500, 800, 1100, and 1400 m s^{-1}, and the dark contours indicate downward velocities with the contour levels of 300, 1500, and 2700 m s^{-1}. The field of view of the figures is the same as in Fig. 3.

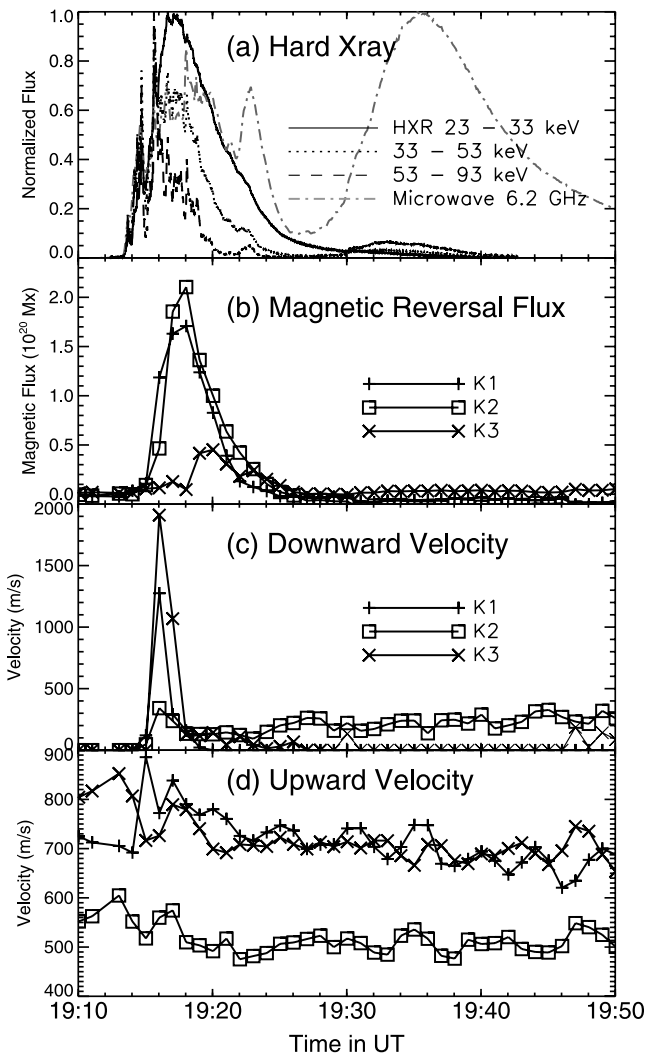

FIG. 5.—(*a*) Hard X-ray and microwave light curves. (*b*) Evolution of the magnetic "reversal" flux (see text) at K1, K2, and K3. (*c*) The rms downward velocity at the flare kernels. (*d*) The rms upward velocity at the flare kernels.

gradual phase of the flare when there occurs another thick-target hard X-ray component with a strong microwave emission, no magnetic anomaly is observed.

Figures 5*c* and 5*d* show the rms downward and upward velocities, respectively. The upward velocity only exhibits a flat trend of order 500–800 m s^{-1}, which is mainly determined by solar rotation. It is seen that at the rise of the impulsive flare emission, a large downward velocity is present and lasts for 1–2 minutes. The strongest downflow, with an rms velocity of 2000 m s^{-1}, occurs in K3, the kernel with the weakest sign reversal. Thus, both the timing and the locations of the downflow are not particularly well correlated with the magnetic anomaly.

3. MDI MEASUREMENTS ON CHANGING LINE PROFILES

It is commonly accepted that measurements of magnetic fields during flares may be greatly distorted as a result of flare-induced line profile changes. In this section we simulate MDI measurements of magnetic fields given a line profile that deviates from the standard quiescent profile in order to see how the change in the profile would modify the measured magnetic signal. For our purpose, certain assumptions and simplifications are made. First, we avoid a comprehensive treatment of line formation and radiative transfer but simply adopt a standard line profile and adjust the profile parameters, namely, the line intensity, line width, and line asymmetry, to simulate the MDI outputs. Second, we adopt a standard Ni I 6768 Å line profile of the quiescent Sun and do not use a line profile specific to a highly magnetized sunspot atmosphere. There are two justifications for this simplification: first, Bruls (1993) has argued that the Ni I line shows minimum profile variation as a function of magnetic field strength, hence we can assume that all variations of the profile are merely a result of other mechanisms such as enhanced heating; second, any magnetic field–dependent signal would lead to a very minor effect on the issue we are investigating, as will be illustrated in the following text. Our simulation serves to qualitatively examine the effect of changing line profiles on the transient sign reversal. For a more rigorous modeling of the MDI output including saturation effects, one should refer to the technical notes by Liu & Norton (2001).

The detailed algorithm that is used by MDI to measure the velocity and magnetic fields is given by Scherrer et al. (1995) and Kosovichev & Zharkova (2001), which is described in the Appendix. Using this algorithm, we alter the shape of the line profiles (see Figs. 6*a*–6*e*, *top panels*) and simulate the MDI measurements of the magnetic fields B_m for each line profile, in comparison with the nominal magnetic field B_n measured from a standard line profile, in order to see how significantly the change in the line profile would affect the measurements.

3.1. *Absorption Profiles*

For absorption profiles, we first look at how the measured magnetic fields change with the line width, given a zero and nonzero (2000 m s^{-1} downward) uniform velocity field, respectively. This case is described in Figure 6*a*. In the top panel, the thin black and gray curves depict line profiles at $B_n = 0$ with and without a velocity field, respectively. A given magnetic field strength will produce a shifted profile at the circular polarization modes. The middle panel gives the measured magnetic field B_m against the nominal fields B_n that is measured from the unmodified standard line profile, and the bottom panel shows the measured velocity fields. When the $B_m \sim B_n$ curve in the middle panel falls in phase I or III, there is not a sign reversal, and when in phase II or IV, a sign reversal will be observed by MDI.

Figure 6*a* shows that for a given magnetic field strength B_n, a narrowed/broadened line results in a greater/smaller B_m. In reality, the existence of turbulence should result in line broadening; hence, the measurement of the magnetic field in a turbulent medium is a lower estimate of the real field, and when the turbulent velocity is large, we expect to see weakened magnetic fields from the measurements. Figure 6*a* also shows that when there is not a velocity field, a significant change ($\geq$10%) due to line broadening can be seen only when the original field strength is greater than 2000 G. A background velocity field of order 2000 m s^{-1} does not lead to a significant modification in the magnetic field measurements below 2000 G. Such experimental results suggest that in active regions close to the disk center,

where the velocity of the solar rotation is small, and where the magnetic fields are not stronger than 2000 G, the measurement error is not significant.

We also investigate cases in which the line profile becomes asymmetric either as a result of the existence of a nonuniform velocity field along the line formation height, i.e., existence of a velocity gradient, or as a result of some complicated radiative transfer process. Observations of asymmetric line profiles are frequently reported in hydrogen lines during flares. Mostly a red asymmetry is reported, which is believed to be due to the so-called chromospheric condensation at the early stage of the flare when an excess pressure front is formed by impulsive heating of the upper chromosphere, which then moves down into the lower atmosphere. To simulate the line asymmetry, we assume that the absorption line is a composite of several shifted absorption components with different velocities, intensities, and line widths. Figure 6*b* displays a few asymmetric line profiles with a varying red shift and the corresponding MDI measurements of the magnetic fields. It is shown, again, that for regions with a smaller field than 2000 G, the measurement error is insignificant. When we add a background uniform velocity field of 2000 m s^{-1}, as may be imposed by solar rotation or flare impact, the measurement error increases but will not show a reversal.

By altering the choices of parameters for absorption profiles, we can produce results similar to those illustrated in Figures 6*a* and 6*b*, where the $B_m \sim B_n$ curve does not fall into region II or IV at any time. The above simulations, therefore, suggest that the observed sign reversal cannot be produced by altering the shape of an absorption line or by adding a moderate velocity field.

In addition, the bottom panels in Figure 6 also show the apparent velocity measured by MDI at given velocities and line profiles. Qualitatively speaking, the results agree with Liu & Norton (2001) that the measurement error in the velocity fields is greater than in the magnetic fields.

3.2. *Emission Profiles*

Patterson (1984) observed magnetic sign reversal using single-channel, filter-based measurements and introduced an emission component to explain the sign reversal. In the case of MDI, the relation between the sign reversal and an emission profile is not so obvious. What measurements MDI may return cannot be readily predicted, but we need to simulate possible types of emission profiles to evaluate the measurements by MDI.

Figure 6*c* shows several profiles turning from absorption to emission. It is evident that when the absorption turns to emission, the measurements severely deviate from the real

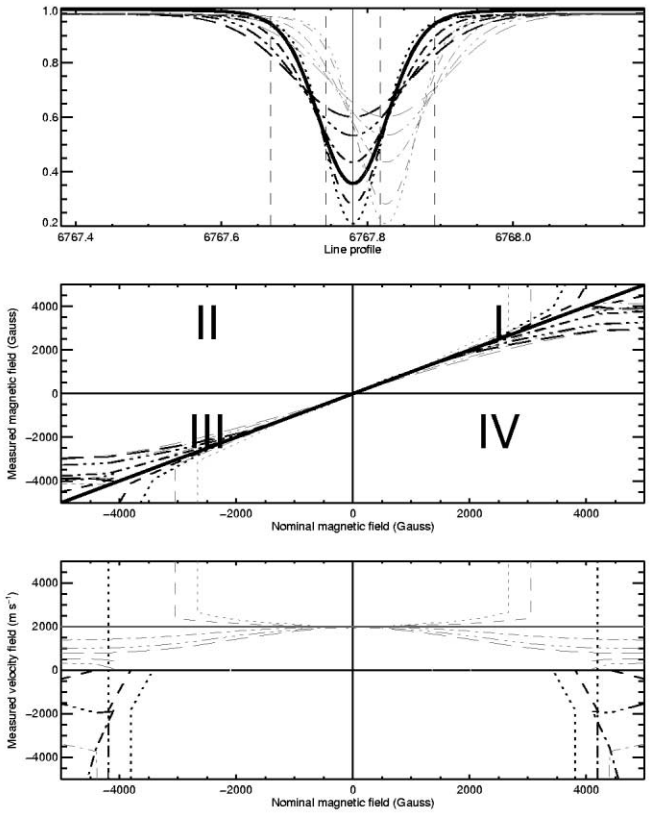

FIG. 6*a*

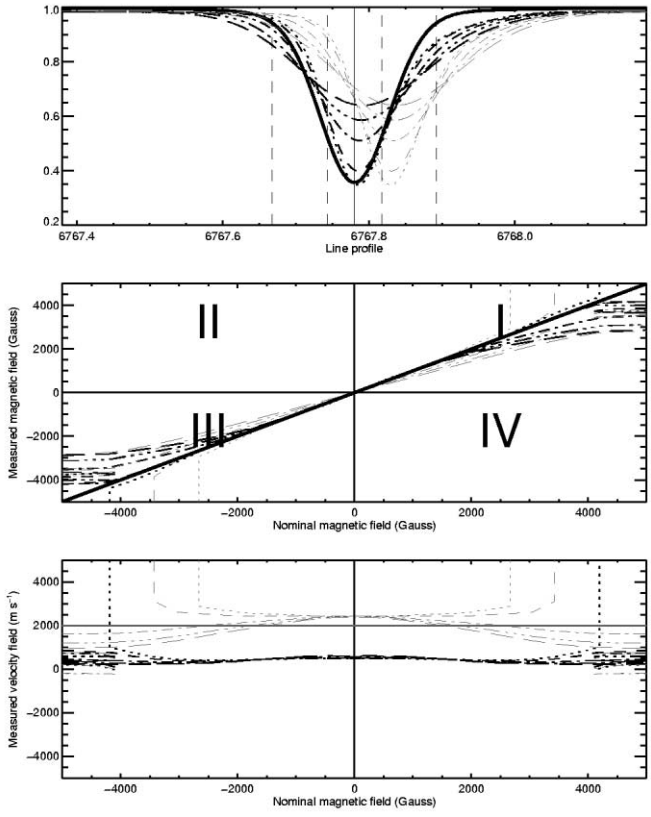

FIG. 6*b*

FIG. 6.—(*a*) *Top*: Thick solid curve gives the standard Ni I line profile in the quiet Sun. The thin curves indicate modified line profiles with a changing line width and with a zero velocity (*black*) and nonzero (*gray*) uniform velocity field with $v = 2000$ m s^{-1} downward. All the displayed line profiles are for the case of $B = 0$ G. *Middle*: Magnetic field strength measured for the modified line profiles given in the top panel against the nominal magnetic field strength measured from the unchanged standard line profile. *Bottom*: Velocity field measured for the modified line profiles given in the top panel against the nominal magnetic field strength measured from the unchanged standard line profile. The gray thick horizontal line indicates the input velocity of 2000 m s^{-1}. (*b*) Same as (*a*), but for the case of a changing asymmetry. (*c*) Same as (*a*), but for the case of emission profiles. (*d*) Same as (*a*), but for the case of centrally reversed narrow profiles. (*e*) Same as (*a*), but for the case of centrally reversed broad profiles.

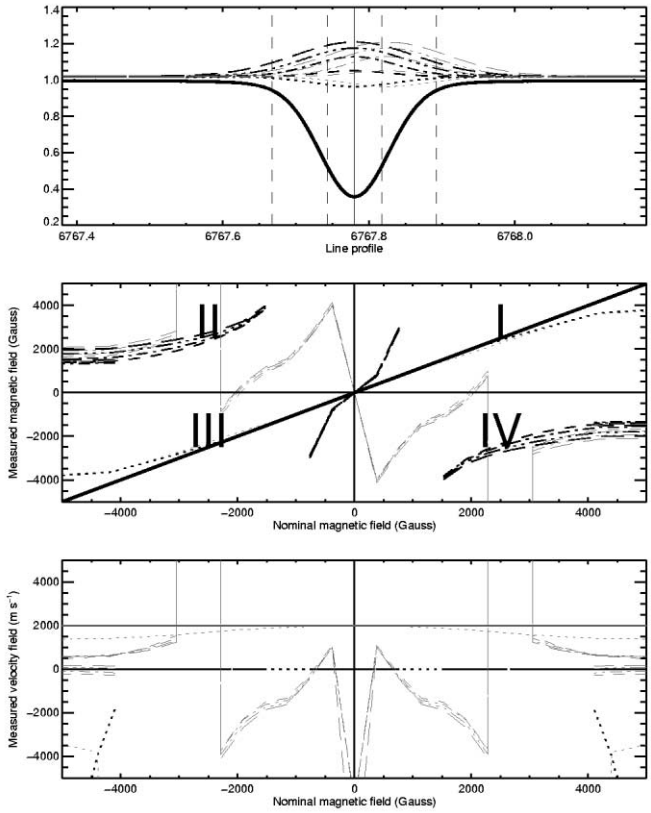

FIG. 6*c*

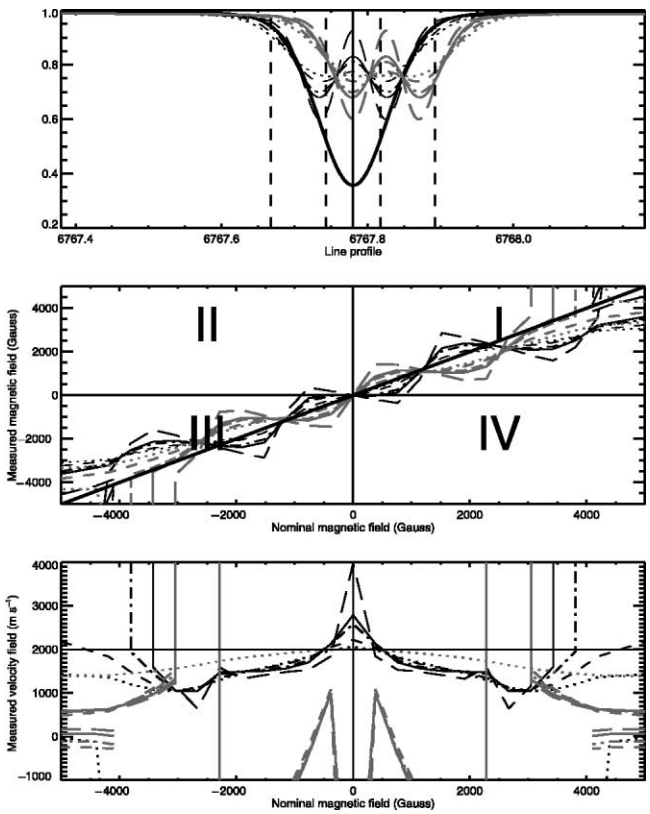

FIG. 6*d*

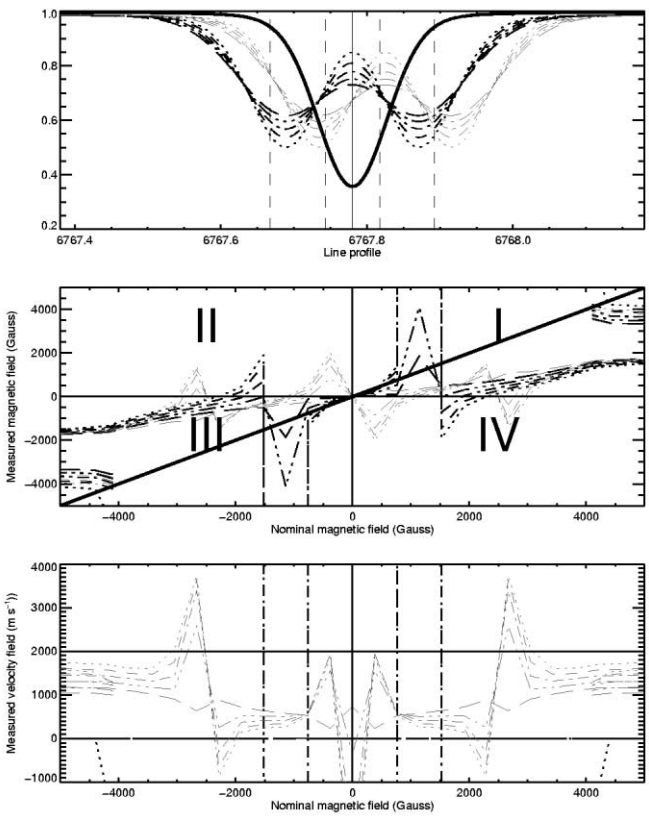

FIG. 6*e*

field, and in strong-field regions ($\geq$1500 G), a sign reversal in the measurement of the magnetic field is unambiguously generated. Given a background velocity field, a sign reversal may be produced also in weak-field regions. Changing the width and asymmetry of the emission profile does not significantly alter the results. Note that a change from an absorption profile into an emission profile considerably distorts the measurements, and if the original magnetic fields are over 1500 G, a larger amount of emission will result in a slightly stronger measured magnetic field with a "reversed" polarity.

The bottom panel of Figure 6*c* also suggests that when the Ni I line turns into emission, the measured velocity field is likely to be sign-reversed as well, if the real velocity field is above $\sim$2000 m s^{-1}.

3.3. *Centrally Reversed Profiles*

In Figures 6*d* and 6*e*, we test some other line profile shapes frequently observed in flare hydrogen lines. Although the Ni I line is a photospheric line that is much more stable than the chromospheric lines, a very large flare like the one presented may produce profiles that deviate severely from normal. When the lower atmosphere is predominantly heated by penetrating nonthermal electron/proton beams or by a warm chromospheric condensation, Hα line profiles may display a central reversal. We simulate such a case by adding to a quiescent absorption component at rest a few emitting components moving at different velocities with a net effect of central reversal.

Figures 6*d* and 6*e* show the cases of central reversal with both "narrow" and "broad" profiles. Comparing Figures 6*d* and 6*e*, it is seen that whether the simulated MDI measurements yield a reversed magnetic field depends on the line width and the intensity of the central reversal. According to the simulation, only when the Ni I line profile is significantly widened to almost twice the original line width and the central reversal component is sufficiently strong can the sign reversal of the magnetic fields be measured in strong-field regions. Given a background velocity field of 2000 m s^{-1}, the sign reversal then preferentially occurs in weak-field regions rather than in strong-field regions.

We note that in umbral areas, even without a flare, the Ni I line shows an evident blend near the line center that can lead to a broadened line profile and a central reversal. However, since a sign reversal has never been discovered in MDI magnetograms in the absence of flares, it is obvious that the blending effects alone cannot provide the required conditions, i.e., a sufficiently strong central reversal in a broadened profile, for a sign reversal to occur in the measured magnetic fields.

3.4. *Summary*

From the simple simulations presented above, we find that a variety of combinations of line profiles and velocity fields may result in the apparent sign reversal in the measured magnetic fields, as long as the strong flare impact on the lower atmosphere results in a sufficient enhancement at the line center. In other words, an effective way to produce the sign reversal of the measured magnetic fields is to convert the absorption profile into an emission profile or to generate a significantly broadened line profile with a strong central reversal.

If the observed magnetic sign reversal is generated by the Ni I line temporarily turning into an emission profile, an apparent sign reversal is also expected to be measured in the velocity fields. In this case, the short duration and misalignment of the observed downward velocities, in comparison with the sign-reversed magnetic anomalies, may be caused by the sign reversal in the measured velocity fields as well. In the case of centrally reversed line profiles, a moderate velocity field would lead to the sign reversal being measured in weak magnetic field regions but not in strong-field regions. Unfortunately, for lack of information of the real velocity fields during the flare, we cannot distinguish the two scenarios. Nevertheless, it is clear that a certain mechanism related to the flare produces significant enhancement of the Ni I line emission at the line center to produce the observed sign reversal in the measured magnetic fields.

We repeat three important facts revealed by the current observations: the apparent sign reversal occurs only in dark, strong-field ($\geq$1000 G) regions within sunspot umbrae, the locations of the anomaly are exactly co-aligned with the thick-target hard X-ray sources, and the transient reversal flux is temporally correlated with the hard X-ray flux. Based on these facts, we propose that at these flare kernels the absorptive Ni I profile is either temporarily turned into an emission profile or significantly broadened with a strong central reversal, as a result of the nonthermal beam impact on the umbral atmosphere.

4. NONTHERMAL BEAM EFFECT ON THE ATMOSPHERE

In this section we briefly discuss the physical implications of the observational facts revealed in this event, namely, the close correlation of the apparent sign reversal with strong magnetic fields, with the dark umbral atmosphere, and with the hard X-ray emission.

The observations and simulations suggest strong emission at the line core of the photospheric Ni I line, which requires a mechanism to significantly enhance the source function for the line. Jones (1989) has shown that the contribution to the formation of the Ni I 6768 Å line center is from the temperature minimum region (TMR), while the source function of the continuum is located in the photosphere and can be approximated by a blackbody Planck function (Bruls 1993). The photospheric temperature of the quiet Sun is about 6000 K, and the temperature of the umbral photosphere is around 4000 K, so that the continuum intensity near the Ni I line in the umbral regions is about 20% of that in the quiet Sun. It is thus seen that, in principle, the energy requirement to turn the absorption line into an emission profile is an order of magnitude smaller than in the case of the quiet-Sun atmosphere. Similarly, the energy requirement for a central reversal is smaller.

Recall that in this event the regions displaying the sign-reversed magnetic anomaly are dark umbral regions with strong magnetic fields, $B \geq 1000$ G. That these are necessary conditions is supported by the case of region K3, where the sign reversal occurs only when K3 evolves into the umbra with strong magnetic fields. We also note that in the earlier events studied by Patterson (1984), only regions of strong magnetic fields exhibit a sign reversal. The rationale of this requirement lies in the double advantages of strong fields. First, the simulations in the last section show that the strong-field regions tend to produce a sign reversal

in the MDI measurements. Second, and more importantly from the energetics point of view, in umbral regions where the continuum intensity is low, it requires less energy to bring the line center, or even the whole line, into emission. Specifically, for the MDI measurements of the sign reversal to be stably correlated with hard X-rays, we propose the scenario of an emission or centrally reversed profile in this event, as was also suggested by Patterson (1984). Note that according to recent work by Ding, Qiu, & Wang (2002), it appears to be possible for the Ni I line to come into emission under the conditions described here.

Our observations of the temporal and spatial coincidence between the apparent sign reversal and the hard X-ray emission argue for a mechanism that is directly related to the nonthermal beam effect. For example, Aboudarham & Henoux (1986) proposed that direct heating of the TMR can be achieved by energetic electrons that penetrate to the TMR. These electrons may also generate, by either direct injection or enhanced nonthermal ionization, extra electrons of order 10^{11} cm $^{-3}$ near the photosphere, so that the H^- heating mechanism becomes viable (Machado, Emslie, & Mauas 1986; Metcalf, Canfield, & Saba 1990). In the following, we examine whether the direct penetration of nonthermal electrons into the deep atmosphere is a valid mechanism to produce the magnetic anomaly in this event.

We analyze the hard X-ray spectrum using the observations obtained by HXT at M1, M2, and H channels to estimate the nonthermal flux that is deposited in the lower atmosphere. The derived power-law index of the nonthermal electrons is illustrated in Figure 7*a*, and the thick-target areas can be estimated from the hard X-ray images (Fig. 1). According to Emslie (1978) and Aboudarham & Henoux (1986), only the electrons with energy greater than a threshold $E_1 \approx 350$ keV at the injection can survive to reach the TMR. Figure 7*b* shows that, in this event, the energy flux F_1 with $E_1 = 350$ keV is about 10^8 ergs cm^{-2} s^{-1} at the maximum of both the impulsive phase and the gradual phase. In Emslie's paper, which does not consider any energy loss or thermal diffusion of electrons before they reach the TMR, i.e., electrons penetrate through a cold target, this amount of energy is carried all the way to TMR. So as a very crude estimate, the upper limit of the energy that can reach the TMR, as directly carried by electrons, is about 10^8 ergs cm^{-2} s^{-1}. For comparison, 10^6–10^7 ergs cm^{-2} s^{-1} was required to heat the quiescent TMR in the flare events analyzed by Machado, Emslie, & Brown (1978).

Figures 7*a* and 7*b* show that during the gradual phase (after 19:30 UT), electrons emitting hard X-rays have a much harder spectrum, and $\geq$350 keV nonthermal electrons carry the same amount of energy flux as during the impulsive phase. The hard X-ray images also reveal that one emission source during the gradual phase is located in the umbra with strong magnetic fields. However, we do not observe a sign-reversed magnetic anomaly during the gradual phase. Furthermore, Figures 7*b* and 7*c* show that apparently the magnetic reversal flux during the impulsive phase does not correlate with the energy flux of $F_1(E_1 = 350$ keV), but it correlates very well with the total energy flux with a much lower cutoff $E_1 = 30$ keV. It is obvious that during the impulsive phase, the overall nonthermal flux at $E_1 \geq 30$ keV is much stronger than during the gradual phase by 1–2 orders of magnitude, which probably better explains why the hard X-rays

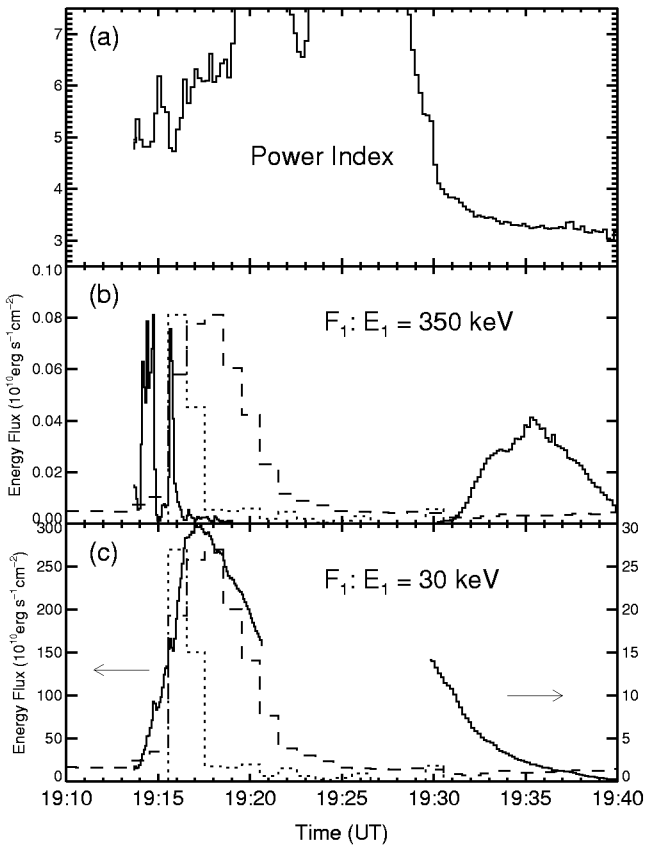

FIG. 7.—(*a*) Power-law index of the electrons derived from the hard X-ray observations. (*b*) Energy flux carried by $\geq$350 keV nonthermal electrons. (*c*) Energy flux by $\geq$30 keV electrons. Note that the scales for the impulsive phase (*left-hand scale*) and for the gradual phase (*right-hand scale*) are different. In both (*b*) and (*c*), the dashed line indicates the magnetic "reversal" flux in K1, and the dotted line indicates the downward velocity in K3, both being arbitrarily normalized.

produce the sign reversal during the impulsive phase but not during the gradual phase.

The above facts serve to exclude the possibility that the TMR be directly heated by $\geq$350 keV electrons that may penetrate that far to produce an emission Ni I profile. For the same reason, the scenario of H^- heating due to enhanced nonthermal ionization or electron injection by penetrating electrons near the photosphere can be rejected. A resolution of the problem may have been found in the recent work of Ding et al. (2002), who modeled the radiative transfer effect on the formation of the Ni I line under the impact of a nonthermal beam using a non-LTE approach. In short, the nonthermal excitation and ionization by penetrating electrons generate a higher electron density that significantly enhances the continuum opacity, pushing the formation height of the line upward. With electrons precipitating and depositing most of the energy in the chromosphere, the enhanced radiation in the hydrogen Paschen continuum gives rise to the line source function, leading to an increase of the line core emission relative to the far wing and continuum. Such nonthermal effects are most pronounced in a cool atmosphere where the continuum is maintained at a low intensity level. Ding et al. (2002) found that in a cool atmosphere, such as the sunspot atmosphere, the precipitation of $\geq$20 keV nonthermal

electrons at the chromosphere can effectively enhance the source function for the Ni I line so as to turn the absorptive line center, or even the whole profile, into emission.

5. OTHER EFFECTS ON MDI MEASUREMENTS

It is known that because of saturation effects, MDI cannot measure properly the strong magnetic fields in umbral regions (Liu & Norton 2001). These include several aspects. First, in the umbral regions, the magnetic field is very strong, resulting in a large Zeeman split that may go beyond the working range of the algorithm. Figure 6 shows that distorted measurements are more likely to be produced in strong-field regions when there are modifications in the absorptive line profiles. This, however, does not lead to a sign reversal. Second, when the light level is low in umbral regions, the measurement in these regions can be greatly contaminated by scattered light from nearby brighter regions, such as penumbral or quiescent regions. In this case, the instrument measures the magnetic fields in penumbral or even quiescent regions, which are also much weaker than in the umbral regions, but the measured magnetic fields will not reverse the sign. Third and most important, in umbral regions where the light level is too low and the effective line depth is substantially reduced, or when the line profile becomes very irregular (such as shown in Figs. 6*d* and 6*e*) so that $F_1 - F_3$ or $F_4 - F_2$ is approaching zero, the MDI onboard algorithm breaks down, leading to the MDI "specific" saturation effects such as shown in Figure 3. However, it remains unclear whether such floating errors by the onboard algorithm applied to complicated line profiles during the flare would generate a lasting sign reversal. To fully understand this issue, it is desirable to obtain more observations of this kind, which also include the Ni I line profiles under flare impact.

It is possible that a sufficiently large velocity field may distort the MDI measurements. It is found that with a velocity of 6 km s^{-1}, the Ni I line will be out of the working range of the algorithm (Liu & Norton 2001), beyond which MDI mainly looks at the far wing of the Ni I line and at best can only detect one of the two Zeeman split components. Simulations similar to those done in § 4 but with a large velocity field reveal that as long as the profile remains absorptive the measurements do not yield a sign reversal unless the velocity is enlarged to near 10 km s^{-1}. In such a case, however, the whole regime from the weak-field to strong-field regions becomes sign-reversed, which cannot explain the observed strong-field preference. The persistence of the observed sign reversal also requires that this large velocity be maintained in the photosphere for about 10 minutes throughout the impulsive phase over all three kernels, which seems unlikely.

6. CONCLUSIONS

In this paper we present observations of a magnetic anomaly in MDI magnetograms during the impulsive phase of an X-class flare. The co-aligned magnetograms and hard X-ray images reveal that a sign-reversed magnetic anomaly occurs in dark umbral regions of strong magnetic field that coincide with the locations of the thick-target hard X-ray emission. The temporal evolution of the magnetic "reversal" flux also correlates well with the hard X-ray light curves. These observational facts provide strong evidence that the apparent magnetic sign reversal is closely associated with the effect of precipitating electrons on the lower atmosphere, preferentially the cool, sunspot atmosphere.

Our simulation of MDI measurements of the Ni I 6768 Å line profile with varying parameters suggests that the observed sign reversals are likely to be produced when the absorption line is centrally reversed, or comes into emission, as a result of the prominent nonthermal impact on the umbral atmosphere of strong magnetic fields. By comparing the nonthermal energy flux during the impulsive phase, when the anomaly occurs, and during the gradual phase, when there is no anomaly, we find that the sign reversal may not be produced by direct penetration of high-energy ($\geq$350 keV) electrons into TMR, but by a comprehensive radiative transfer effect in the umbral atmosphere under the impact of a nonthermal beam. The above scenario is confirmed by the non-LTE calculations of the Ni I 6768 Å line in Ding et al. (2002).

As a side remark, we also note that in regions with strong magnetic fields, MDI measurements show saturation effects due to low umbral light levels, scattered light, and, most importantly, failure of the onboard algorithm when it is applied to low intensity and irregular line profiles. It remains unclear and thus deserves further investigation how these instrumental effects could result in a flare-related sign reversal. A large velocity field generated by flare energy release could in principle yield false measurements including a sign reversal, but it would require an unphysical photospheric velocity field of over 10 km s^{-1}, persistent through the entire impulsive phase of the flare. Therefore, the scenario of an emission or strong central-reversal profile provides the simplest viable interpretation of the sign reversal in this event from both the observational and theoretical point of view.

The authors thank the *Yohkoh* and MDI teams for data support. We appreciate instructive comments by Y. Liu and A. Kosovichev and helpful discussions with H. Wang and M. D. Ding. We thank the referees for critical comments that helped improve the manuscript substantially. This work is supported by NASA grant NAG5-10212. The OVSA is supported by NSF grant AST 99-87366 to the New Jersey Institute of Technology.

APPENDIX

ALGORITHM OF MDI MEASUREMENTS

The MDI instrument measures the line intensities at five positions along the spectral profile, and at each position, the left and right circular polarization modes are tuned in alternatively. In the top panels in Figures 5*a*–5*e*, the standard quiet-Sun profile is shown by the thick, solid curve, with the solid vertical line indicating the position of the line center and the dashed vertical lines indicating the central positions of four bandpasses along the spectrum from the blue to red side of the line core, at

which the line intensities $F_1 \ldots F_4$ are read out. The four positions are evenly separated by an interval of 0.075 Å. The instrument then performs an onboard algorithm to compute the line shift parameter $\alpha_{l,r} = (F_1 + F_2 - F_3 - F_4)/(F_1 - F_3)$ when the numerator is positive or $\alpha_{l,r} = (F_1 + F_2 - F_3 - F_4)/(F_4 - F_2)$ when the numerator is negative, with $F_1 \ldots F_4$ measured at left and right circular polarization modes, respectively. The line profile is convolved with the MDI instrument profiles before reading out $F_1 \ldots F_4$ (A. Kosovichev 2002, private communication). The line shift parameter is then converted to the velocity using an empirical lookup table (see Scherrer et al. 1995). The mean of and difference between the two velocities derived at the left and right circular modes are returned as the measured velocity and magnetic field strength, respectively, i.e., $V_m = (V_l + V_r)/2$ and $B_m = (V_l - V_r)/2.84$. Only the final results are returned from MDI, while the intermediate quantities, like the line intensities at five positions and the shift parameters, are not recorded once the computation is done. Analytically speaking, given a linear approximation, i.e., weak (magnetic/velocity) field approximation, the algorithm devised for MDI minimizes the sensitivity of the measurements to change of line profiles. This can be also seen in the text in which we simulate the MDI measurements on various sorts of line profiles.

REFERENCES

Aboudarham, J., & Henoux, J. C. 1986, A&A, 156, 73
Bruls, J. H. M. J. 1993, A&A, 269, 509
Ding, M. D., Qiu, J., & Wang, H. 2002, ApJ, 576, L83
Emslie, A. G. 1978, ApJ, 224, 241
Gary, D. E., & Hurford, G. J. 1990, ApJ, 361, 290
Handy, B. N., et al. 1999, Sol. Phys., 187, 229
Jones, H. P. 1989, Sol. Phys., 120, 211
Kosovichev, A. G., & Zharkova, V. V. 2001, ApJ, 550, L105
Kosugi, T., et al. 1991, Sol. Phys., 136, 17
Liu, Y., & Norton, A. A. 2001, MDI Measurement Errors: The Magnetic Perspective/SOI-Technical Note 01-144
Machado, M. E., Emslie, A. G., & Brown, J. C. 1978, Sol. Phys., 58, 363
Machado, M. E., Emslie, A. G., & Mauas, P. J. 1986, A&A, 159, 33
Metcalf, T. R., Canfield, R. R., & Saba, J. L. R. 1990, ApJ, 365, 391
Patterson, A. 1984, ApJ, 280, 884
Patterson, A., & Zirin, H. 1981, ApJ, 243, L99
Qiu, J., Lee, J., & Gary, D. E. 2003, ApJ, submitted
Sakurai, T., & Hiei, E. 1996, Adv. Space Res., 17(4/5), 91
Scherrer, P. H., et al. 1995, Sol. Phys., 162, 129
Wang, H., Spirock, T. J., Qiu, J., Ji, H., Yurchyshyn, V. B., Moon, Y.-J., Denker, C., & Goode, P. 2002, ApJ, 576, 497
Zirin, H., & Tanaka, K. 1981, ApJ, 250, 791